Yeganeh, Maryam; Akram, Muhammad Saad; Cheng, Qiang; Karimkashi, Shervin; Kaario, Ossi; Larmi, Martti

Experimental study of hydrogen jet dynamics : Investigating free momentum and impingement phenomena

Published in:
International Journal of Hydrogen Energy

DOI:
10.1016/j.ijhydene.2024.04.296

Published: 28/05/2024

Document Version
Publisher's PDF, also known as Version of record

Please cite the original version:
Yeganeh, M., Akram, M. S., Cheng, Q., Karimkashi, S., Kaario, O., & Larmi, M. (2024). Experimental study of hydrogen jet dynamics : Investigating free momentum and impingement phenomena. *International Journal of Hydrogen Energy*, *68*, 1423-1437. https://doi.org/10.1016/j.ijhydene.2024.04.296

International Journal of Hydrogen Energy 68 (2024) 1423–1437

Contents lists available at ScienceDirect

International Journal of Hydrogen Energy

journal homepage: www.elsevier.com/locate/he

Experimental study of hydrogen jet dynamics: Investigating free momentum and impingement phenomena

Maryam Yeganeh [*], Muhammad Saad Akram, Qiang Cheng, Shervin Karimkashi, Ossi Kaario, Martti Larmi

Department of Mechanical Engineering, Aalto University, School of Engineering, 02150, Espoo, Finland

ARTICLE INFO

Handling Editor: Umit Demirci

Keywords:
H_2 jet
Z-type schlieren
Nozzle geometry
Injection angle
Pressure ratio
Injection duration

ABSTRACT

There is a growing interest in the utilization of hydrogen (H_2), as a zero-carbon fuel, in internal combustion engines (ICEs). Accordingly, the primary focus of this study is to investigate low-pressure H_2 jet dynamics, which play a vital role in air-fuel mixing especially in direct injection (DI) engines. High-speed z-type schlieren imaging is employed in a constant volume chamber to study the effect of nozzle geometry (single-hole, double-hole, and multi-hole), pressure ratios (PR = injection pressure (P_i)/chamber pressure (P_{ch})), injection angle (10°, 15°, and 20°), and injection duration (ID) on the H_2 jet characteristics. Image post-processing is executed in MATLAB and Python to extract the H_2 jet characteristics, including penetration and cross-sectional area. The novelty stems from the comprehensive investigation of H_2 jet dynamics and impingement phenomenon under various engine-like conditions. The results indicate that apart from the fact that higher pressure ratios (PRs) improve the air-fuel mixing, the single-hole nozzle induces the fastest H_2 jet penetration and the smallest cross-sectional area. Conversely, the double-hole nozzle leads to the slowest penetration and the most expansive cross-sectional area. The performance of the multi-hole nozzle falls between that of the single-hole and double-hole nozzles. Additionally, changing the injection angle results in jet-piston impingement at the periphery, leading to higher H_2 concentration in those areas. This negatively affects the formation of an optimal air-fuel mixture. It is also found that changing the injection duration (ID) has no noticeable impact on the H_2 jet's behavior.

1. Introduction

As the world seeks sustainable and environmentally friendly energy solutions [1,2], the interest in using H_2 as a viable fuel for ICEs has gained a significant momentum. Utilizing H_2 in ICEs is of high interest for multiple reasons. First, H_2 is a carbon-free fuel, and it offers the potential to reduce greenhouse gas emissions [3]. Second, the existing infrastructure and expertise related to ICEs may offer valuable insights for the integration of H_2-powered vehicles, albeit with some potential transitional challenges [4–10]. Third, H_2 engine offers the advantage of swift refueling and an extensive driving range, rendering it well-suited for applications necessitating rapid refueling and prolonged travel distances. Lastly, H_2 can be produced from diverse sources, including renewable energy such as solar, wind, or hydroelectric [11,12], contributing to energy security, and reducing dependence on fossil fuels.

In the development of H_2 ICEs, unique chemical and physical properties of H_2 present both opportunities and challenges [13]. On one hand, H_2's broad flammability range allows for lean combustion, resulting in improved thermal efficiency and reduced high-temperature NOx emissions. Additionally, its high specific energy density increases energy output per unit mass, complemented by its low molecular weight and high diffusivity that facilitate efficient mixture formation. On the other hand, challenges associated with H_2's properties, such as low density and susceptibility to pre-ignition and knocking, need to be carefully addressed. Moreover, the combination of a low quenching distance and high flame propagation speed can lead to backfire and combustion heat loss. With comprehensive solutions that effectively balance the advantages and address the limitations, the overall outlook for H_2 ICEs is promising for the transition towards a sustainable transportation future.

Given the promising attributes of H_2 ICEs, it becomes imperative to optimize their operation. One critical aspect of this optimization lies in injection parameters, as they can significantly influence air-fuel mixing and subsequently combustion characteristics. In this context, ICEs are

* Corresponding author.
E-mail address: maryam.yeganeh@aalto.fi (M. Yeganeh).

https://doi.org/10.1016/j.ijhydene.2024.04.296
Received 21 December 2023; Received in revised form 19 April 2024; Accepted 25 April 2024
Available online 8 May 2024

typically classified into two categories based on fuel injection method: port fuel injection (PFI) and direct injection (DI) each utilizing various ignition techniques such as spark ignition (SI) or dual-fuel (DF) operation [14–18]. DI offers several advantages over PFI, including precise fuel delivery into the combustion chamber, leading to improved combustion efficiency, reduced fuel consumption, and increased power output [19–23]. Furthermore, DI engines provide superior air-fuel mixing, resulting in enhanced power and torque output, increased resistance to knocking, and reliable cold start performance [24–31].

However, challenges persist regarding emissions from H_2 DI engines [31–33]. High combustion temperatures at locally rich regions may lead to NOx formation in the exhaust. In addition, the necessary lubrication of moving parts in these engines introduces the possibility of hydrocarbon (HC) emissions if oil leaks or burns incompletely [32]. The dynamics of the gaseous H_2 jet can also play a significant role in the formation of particulate matter and gaseous pollutants [34]. According to Holtzer and Tartakovsky [34], H_2 gas jet depicts a three-zone behavior -the free-jet, impinging region, and climbing jet vortex-of which the latter is responsible for involvement of the lubricant in combustion.

In light of the preceding context, optimizing injection parameters and investigating the H_2 jet dynamics are both key elements in the development of H_2 DI engines. Hence, this study aims to investigate the impact of various injection-related parameters on the characteristics of low-pressure H_2 jets since understanding the jet dynamics provides valuable insights into air-fuel mixing and, consequently, combustion process. It should be also noted that injection pressures are generally categorized into three ranges: low-pressure (<5 MPa), medium-pressure (5–10 MPa), and high-pressure (>10 MPa), although definitions can vary across different sources [18,33,35]. In this study, we also define low-pressure as <5 MPa, consistent with our injection pressure of 2.5 MPa.

It is also important to highlight the benefits of low-pressure injection compared to high-pressure injection. While high-pressure injection offers advantages such as enhanced fuel mass flow control, improved hydrogen jet penetration, and potentially higher power output, it also requires robust components, adding complexity and cost while raising safety concerns. Space limitations in certain engine designs may also restrict the installation of high-pressure components. For applications prioritizing fuel efficiency over power output, low-pressure injection can be beneficial by reducing cooling losses, as well. Recent findings of [36] also highlight the superior combustion performance of low-pressure over high-pressure injection in H_2DI engines, emphasizing the need for further research in low-pressure H_2DI engines.

Another key aspect in H_2DI engines is the preparation of gaseous fuel mixture, which is inherently slower than that of liquid fuels due to gas' lower momentum transfer capability [37]. This presents a significant challenge in achieving effective fuel delivery into the combustion chamber, underscoring the importance of comprehending gas jet behavior in advancing H_2 DI engines. In the following, the most relevant literature on H_2 gas jets characteristics, mixing phenomenon in engines, and numerical simulations related to either H_2 jets or mixing in engines are presented with particular emphasis on H_2 gas jets characteristics.

With respect to H_2 gas jet characteristics, Lee et al. [38] investigated the H_2 gas jet dynamics at various ambient pressures. In their study, a high-pressure H_2 jet at 10 MPa was visualized in a constant volume combustion chamber with varying ambient pressures and injection durations. Utilizing the schlieren method with a high-speed camera, they captured the characteristics of the H_2 hollow-cone jet. Their findings revealed that high ambient pressure led to reduced vertical jet penetration and area. Additionally, increased ambient pressure resulted in greater heterogeneity of the mixture. In a following work, Lee et al. [39] studied the behavior of H_2 jets through a similar experimental approach as well as numerical simulations. They visualized the H_2 jet vapor intermittency and vortex structure and demonstrated the aerodynamics of the jet through numerical simulations, revealing vortical flow formation in the inner core region where the pressure was relatively lower compared to the outer side. Their investigation into injection strategies also indicated that multiple injections were more effective in achieving a proper H_2-air mixture near the spark plug than a single injection.

Coratella et al. [40] studied the characteristics of H_2 jets from outward-opening injectors using high-speed schlieren imaging, focusing on the combined effects of backpressure and pintle dynamics on jet development. Lower backpressures resulted in faster jet penetrations, accelerated by increased current intensity due to faster pintle motion and stronger rarefaction waves aiding H_2 flow momentum. Additionally, increased current intensity expanded jet area and volume under constant ambient pressure. In another study by Zhao et al. [41], the microscopic characteristics of H_2 jets from outward-opening injectors and their effects on gas-air mixing were investigated. They noted a decrease in jet asymmetry as it developed, eventually stabilizing once the valve was fully open. This stabilization was further enhanced by increased ambient pressure. The outward-opening injector exhibited greater stability compared to a single-hole injector. They also found that gas concentration varied along the jet's axial direction, with stabilization occurring at greater axial penetrations, and the equivalent ratio settling into a stable range. Furthermore, Wang et al. [26] studied the characteristics of H_2 jets from an outward-opening injector using high-speed schlieren imaging in a constant volume chamber across a range of pressure ratios (PRs) from 10 to 140. They observed that the jet forms a conical shape near the injector and evolves into a spherical vortex further downstream. As PR increased, the jet's axial and radial penetration as well as its volume also increased. The jet spread angle was largely consistent across PRs, except at lower PRs.

In the context of H_2 jet mixing phenomenon in engines, Koyanagi et al. [42] explored the impact of H_2 jet on mixture formation in a high-pressure H_2 DISI engine. They found that higher injection pressures improved jet penetration while reduced H_2 diffusion near the spark gap. Moreover, Wallner et al. [43] studied injection parameters in a H_2 DI engine and observed that injection timing and optimizing nozzle design played a vital role in engine NOx emissions. Salazar and Kaiser [44,45] investigated mixture uniformity in a H_2 DI optical engine with varying injection timings and revealed that early injections resulted in more uniform mixtures. More recently, Lee et al. [46] assessed the impact of different mixing modes on a H_2 DI engine efficiency and emissions. They noted that the lean-stratified charge (LSC) mode maximized thermal efficiency under low loads, while stratified rich H_2 led to increased NOx emissions.

There have been also several numerical studies on H_2 jets or their mixing behavior in engines over the past few years. In an LES study by Hamzehloo et al. [47], turbulent under-expanded H_2 and CH_4 jets were examined at different nozzle pressure ratios and ambient pressures, including the elevated pressures relevant to DI ICEs. They found that higher nozzle pressure ratios or ambient pressures led to locally richer mixtures. In another study, Qu et al. [48] conducted a 3D CFD simulation of an H_2 DISI engine and identified turbulence intensity and injection penetration distance as the key factors impacting mixture homogeneity. Moreover, Wu et al. [49] utilized unsteady RANS simulations to explore air-fuel mixing in a H_2 DI optical engine. The findings revealed that high-pressure injection coupled with sufficient fuel residence time could significantly influence air-fuel mixing.

In line with the provided literature review, further research is required to understand H_2 jet characteristics and mixing behavior under the effect of influential parameters such as injection pressure, timing, orientation, and nozzle geometry, to advance the development of future H_2 DI engines. In particular, a comprehensive investigation of all the mentioned influential parameters for low-pressure H_2 jets is lacking from the literature. More importantly, injection angle effect on H_2 jet mixing in DI engines is not thoroughly investigated. In this respect, a confidential and novel low-pressure H_2 injector and a new piston bowl profile for a prototype H_2 DI engine have been designed and tested.

In order to fill the specified knowledge gap, the main objective of this study is to assess the impact of four key parameters - nozzle geometry (single-hole, double-hole, and multi-hole), pressure ratio (PR = injection pressure (P_i)/chamber pressure (P_{ch}) = 25, 10, 5, and 2.5), injection angle (10°, 15°, and 20° with respect to the piston liner), and injection duration (ID = 2 & 3 ms) - on a low-pressure H_2 jet characteristics i.e., H_2 jet penetration (the distance along the jet axis to the jet boundary) and the cross-sectional area (the region enclosed within the jet boundaries).

The remainder of the paper is organized as follows. In Section 2, the experimental set-up and methodology are explained. Section 3 presents a systematic analysis of the impact of variables, including nozzle geometry, pressure ratio (PR), injection angle, and injection duration (ID), on the dynamics and characteristics of the H_2 jet. Lastly, Section 4 contains the presentation of summary and conclusions.

2. Experimental setup and methodology

This section provides a comprehensive description of the experimental setup and optical system, the test matrix, image post-processing techniques, and error analysis methods employed in the study.

2.1. Experimental setup and optical system

During the experimental campaign, two different sets of measurements were conducted to investigate the impact of specific parameters on the H_2 jet characteristics. The first set aimed to assess the effect of nozzle geometry (single-hole, double-hole, and multi-hole), pressure ratio (PR) and injection duration (ID) in free momentum propagation phase, while the second set focused on analyzing the injection angle and jet-wall impingement. The first set of measurements involved using the injector with three different caps (single-hole, double-hole, and multi-hole), all having identical total cross-sectional area and mass flow rate. In contrast, the second set of measurements only employed the single-hole cap. It should be also noted that the impact of ID was examined solely for the single-hole nozzle at a single PR.

For both sets of measurements, a constant volume chamber with optical access through lateral windows was used. The chamber was connected to a nitrogen bottle rack for pressurization and a H_2 bottle for the injection line towards the injector. The injector utilized in the experiments was a BOSCH solenoid outward-opening gas injector designed specifically for low pressure H_2 injection at 2.5 MPa. The injector was mounted at the top center and in a vertical orientation. Consequently, investigating the effect of the injection angle was accomplished by placing a sample of a piston bowl profile with three different angles at the bottom of the chamber. This approach was adopted as an alternative to altering the real injector angle due to the safety concerns.

Fig. 1 depicts the experimental setup and highlights the differences between the first and second sets of measurements (H_2 jet's free momentum (1) and impingement analysis (2)). Additionally, the setup was equipped with an exhaust line, comprising a regulating valve to align the chamber pressure with the gas supply, a shut-off valve for chamber venting, and a relief valve to release pressure once the maximum chamber pressure was reached.

To visualize the H_2 jet, high-speed z-type schlieren imaging was employed to detect the density gradient of the jet [50]. Fig. 2 presents a schematic of the schlieren imaging setup. As it is shown, the jet is first illuminated by either a high-speed laser or LED light source and a parabolic mirror, which leads to light refraction. Another parabolic mirror then focuses the beam onto the lens of the high-speed camera. To generate the schlieren image, an iris is placed in front of the camera, selectively blocking the refracted light. More detailed characteristics of the optical system are listed in Table 1.

The control system was powered by LabVIEW software and driver from National Instrument [51]. The primary functions of the control system were twofold: (1) synchronizing the injector, high-speed camera (Phantom V2012 [52]/Photron FastCam SA-Z [53]), and the laser light source (CAVILUX smart laser C006 [54]) (2) efficiently controlling and monitoring the injection pressure, chamber pressure, and temperature throughout the experiments. It is worth mentioning that the first set of experiments used a laser light source and the Phantom monochrome camera whereas the second set utilized the Photron SA-Z color camera and a continuous LED light source that did not require control by the

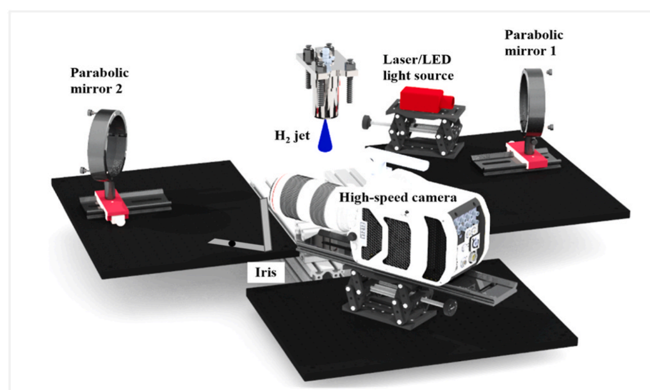

Fig. 2. A schematic picture of the z-type schlieren imaging system used in the experimental measurements.

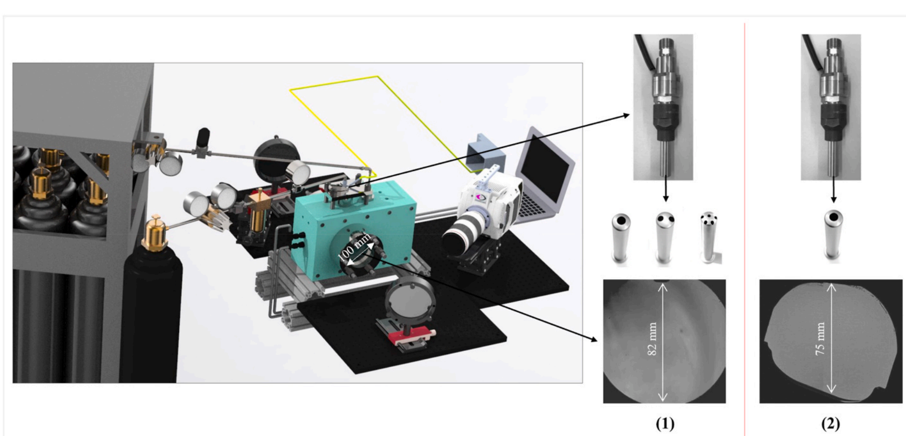

Fig. 1. A schematic picture of the experimental setup. Subfigure (1) shows the injector caps (single-hole, double-hole, and multi-hole) and an inside view of the chamber window in the first set of measurements. Subfigure (2) displays the single-hole injector cap (single-hole) and an inside view of the chamber window with the piston bowl profile at the bottom in the second set of measurements.

Table 1
Optical system components.

Component	Feature
CAVILUX smart laser C006	640 nm
LED	21 KW
Frame Rate of the Phantom camera	34000 fps
Resolution the Phantom camera	768*768
Exposure time of the Phantom camera	2 µs
Frame Rate of the Photron Camera	40000 fps
Resolution of the Photron Camera	768*640
Shutter speed of the Photron Camera	1/800000 s
Focal length of the first parabolic mirror	609,6 mm
Focal length of the second parabolic mirror	762 mm
Percentage of the knife-edge cut-off	Approximately 60%

control system.

2.2. Test matrix

Table 2 presents the test matrix to assess the jet characteristics i.e., the jet penetration and cross-sectional area under the effect of nozzle geometry (single-hole, double-hole, and multi-hole), pressure ratio (PR = injection pressure (P_i)/chamber pressure (P_{ch}) = 25, 10, 5, and 2.5), injection angle (10°, 15°, and 20°), and injection duration (ID = 2 & 3 ms). The experiments were performed at the standard room pressure (0.1Mpa) and temperature (300K). As mentioned earlier, the injection pressure (P_i) was maintained at 2.5 MPa for all the measurements, and a minimum of 20 repetitions were conducted for each test point to ensure the data accuracy. Additionally, to account for potential variations in the jet behavior between different repetitions (jet-to-jet variations), image similarity analysis was executed to verify the adequacy of the number of repetitions.

Table 2
Experimental matrix for free momentum and impingement studies.

No. \Variable	Nozzle geometry	Injection angle	Pressure Ratio	Injection Duration
Case 1	Single-hole	–	25, 10, 5, 2.5	3 ms
Case 2	Double-hole	–	25, 10, 5, 2.5	3 ms
Case 3	Multi-hole	–	25, 10, 5, 2.5	3 ms
Case 4	Single-hole	10°, 15°, 20°	25	3 ms
Case 5	Single-hole	10°, 15°, 20°	10	3 ms
Case 6	Single-hole	10°, 15°, 20°	5	3 ms
Case 7	Single-hole	10°, 15°, 20°	2.5	3 ms
Case 8	Single-hole	–	25	2,3 ms

2.3. Image post-processing

The image-processing for the H_2 jet free momentum measurements were conducted with a custom MATLAB code. The post-processing steps for calculating the jet characteristics (penetration and cross-sectional area) are shown in Fig. 3. To define the jet characteristics, notably, jet penetration signifies the distance along the jet axis to the jet boundary, while the jet cross-sectional area specifies the region enclosed within the jet boundaries.

To further estimate the jet-to-jet variations, a custom Python code was developed to analyze the structural similarity index metric (SSIM) [55] between different repetitions of each test point. The SSIM quantifies the perceived similarity between two images by considering structure and its values range from 0 to 1(100%), where 0 indicates no similarity and 1(100%) indicates perfect similarity. Fig. 4 displays the SSIM for the worst-case scenario in the measurement campaigns, representing the minimum similarity among all the repetitions of a test point. The minimum similarity, approximately 0.8 (80%), occurs at the jet-wall impingement due to the increased pixel grayscale differences,

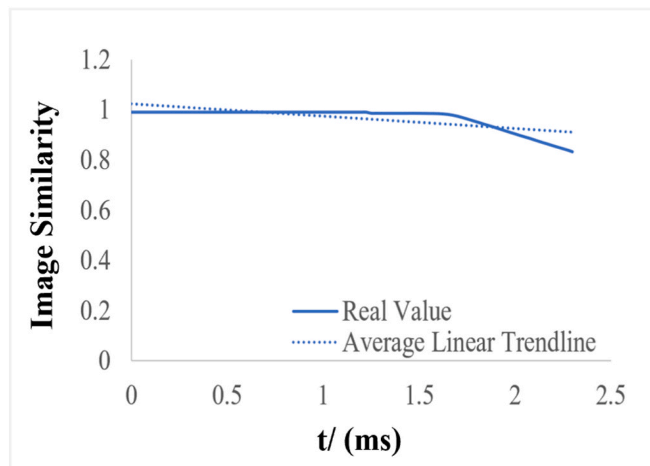

Fig. 4. The image similarity analysis using the custom Python code.

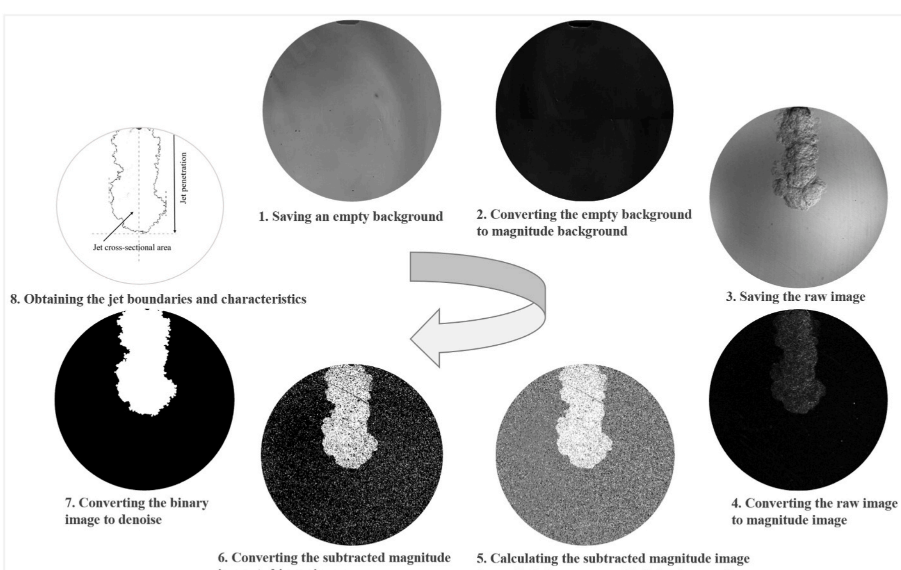

Fig. 3. The image post processing steps followed in the custom MATLAB code.

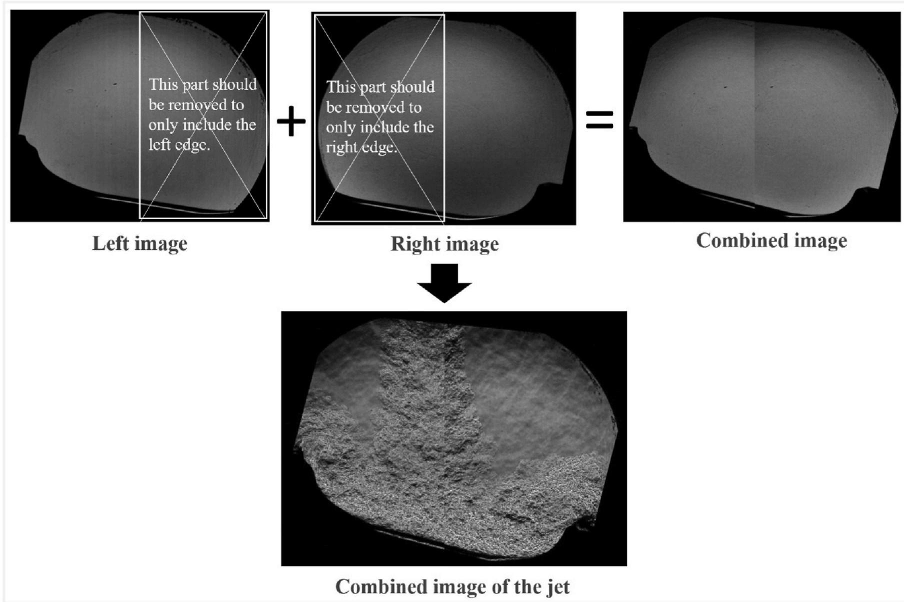

Fig. 5. Combining the left and right-hand side views to generate a combined/complete image of the jet.

(a) Single-hole jet evolution

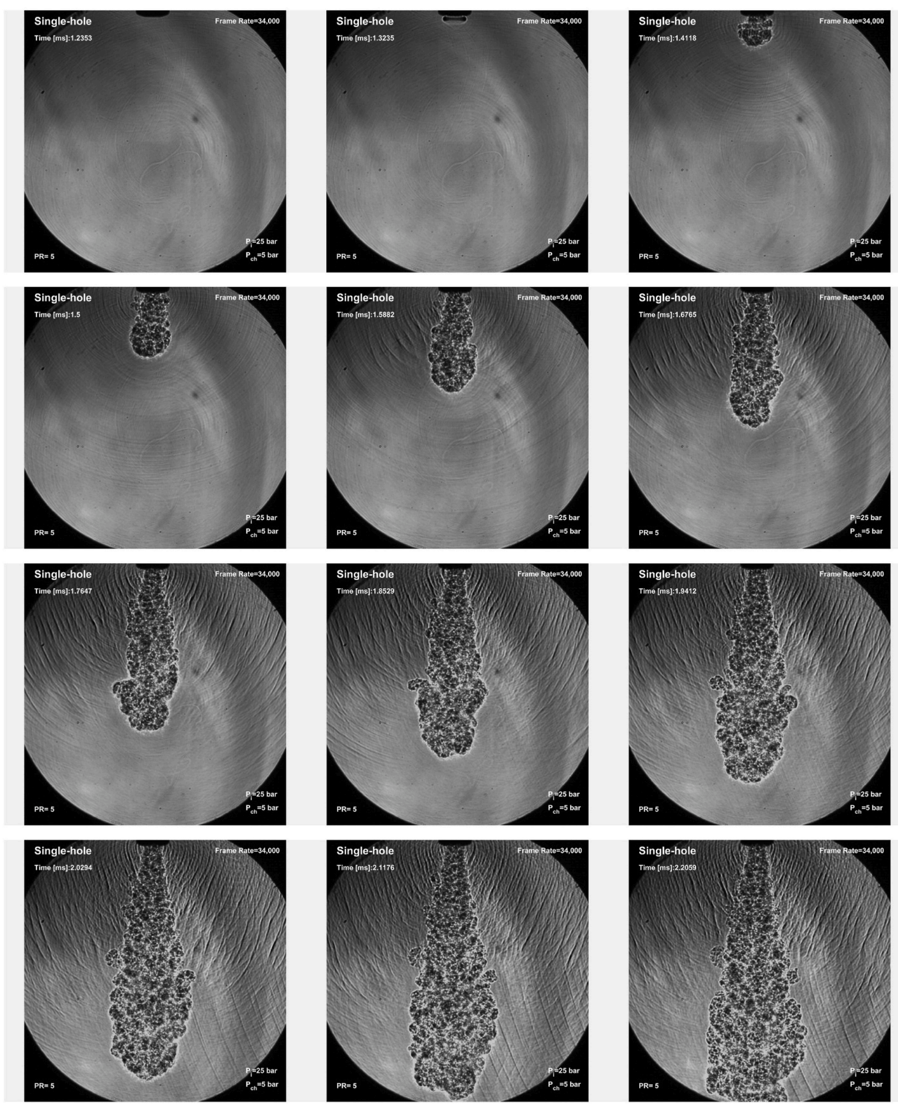

Fig. 6. H_2 jet evolution from the (a) single-hole (b) double-hole & (c) multi-hole nozzle at PR = 5 .

(b) Double-hole jet evolution

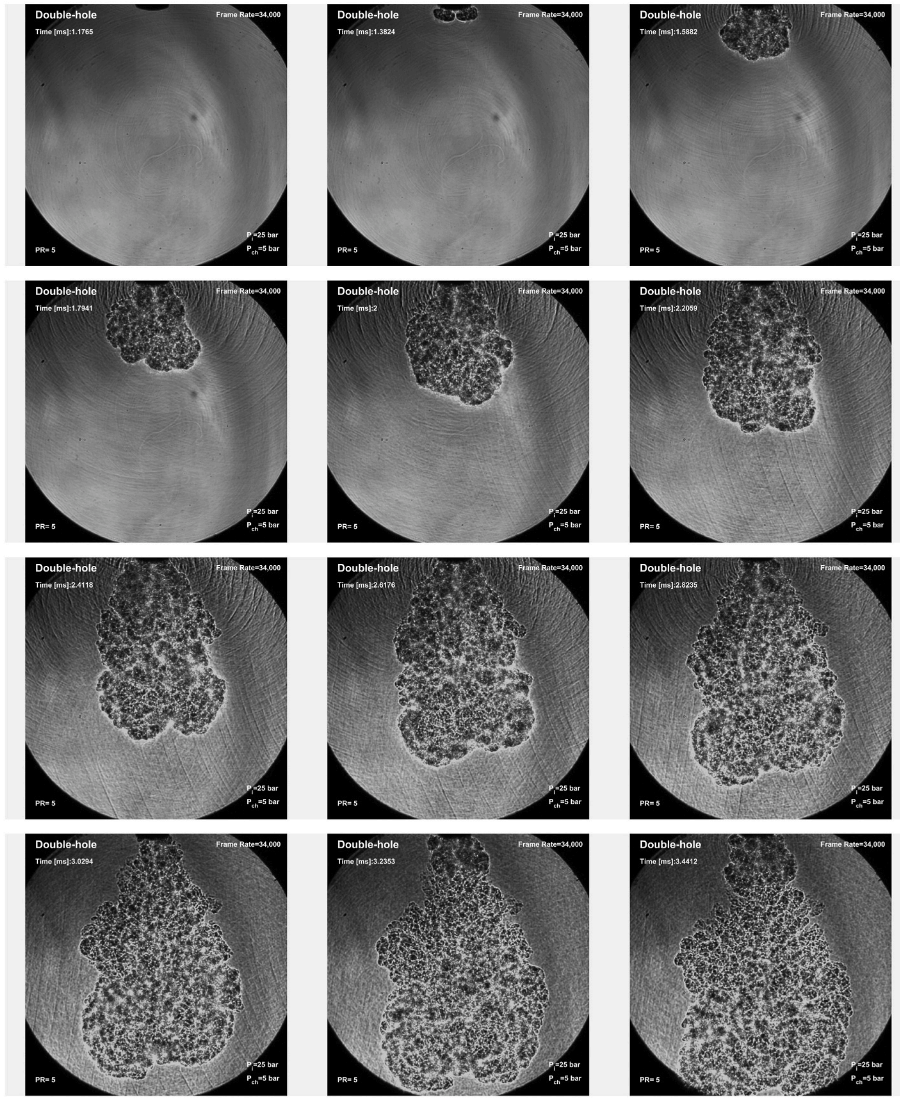

Fig. 6. (*continued*).

aligning logically with the turbulence observed.

For post-processing of the H_2 jet impingement images, a three-step method was employed to analyze the impact of the injection angle as shown in Fig. 5. It is noted that since the window size is smaller than the piston diameter, separate measurements were conducted for the right and left sides. Hence, to obtain a complete view of the jet-wall impingement, first, merging the images of the left and right sides of the jet is needed. Subsequently, the identical steps employed in the free momentum measurements were pursued to calculate the jet characteristics and conduct the image similarity analysis.

2.4. Error analysis

In the context of the present experimental framework, numerous factors contribute to potential sources of error that may impact the precision of the data. Foremost among these factors are the accuracy of the pressure sensors that measure injection and chamber pressures. It is important to acknowledge that the pressor sensors measure gauge pressures by a $\pm 0.5\%$ margin of error concerning full-scale output accuracy. Furthermore, the injector undergoes pressure gradients, characterized by a minimum pressure drop of 0.1 MPa occurring immediately prior to the injector valve during the injection phase. This pressure discrepancy is coupled with internal losses attributed to the intermediate space lying between the valve and the cap.

Post-processing captured images in MATLAB introduces an additional layer of complexity. It is important to highlight that the calculation of the jet penetration and cross-sectional area is confined within 95% of the maximum jet penetration. In other words, a 5% margin of error exists in the precision of tracking the jet boundaries.

Lastly, it is imperative to address the potential error stemming from jet-to-jet variations. According to the SSIM analysis, the jet-to-jet variations can reach a maximum value of 20% (Fig. 4). To demonstrate this discrepancy, error bars have been incorporated into the plots that depict jet characteristics i.e., penetration and cross-sectional area in the results section. However, to maintain image clarity, error bars are displayed at intervals of every 3–6 repetitions, rather than for each individual repetition.

3. Results and discussions

In this section, the outcomes of the experimental campaign are presented. Firstly, the influence of nozzle geometry and pressure ratio (PR) on the structure and characteristics of the H_2 jet are investigated. Subsequently, the impact of the injection angle on H_2 jet mixing, from

(c) Multi-hole jet evolution

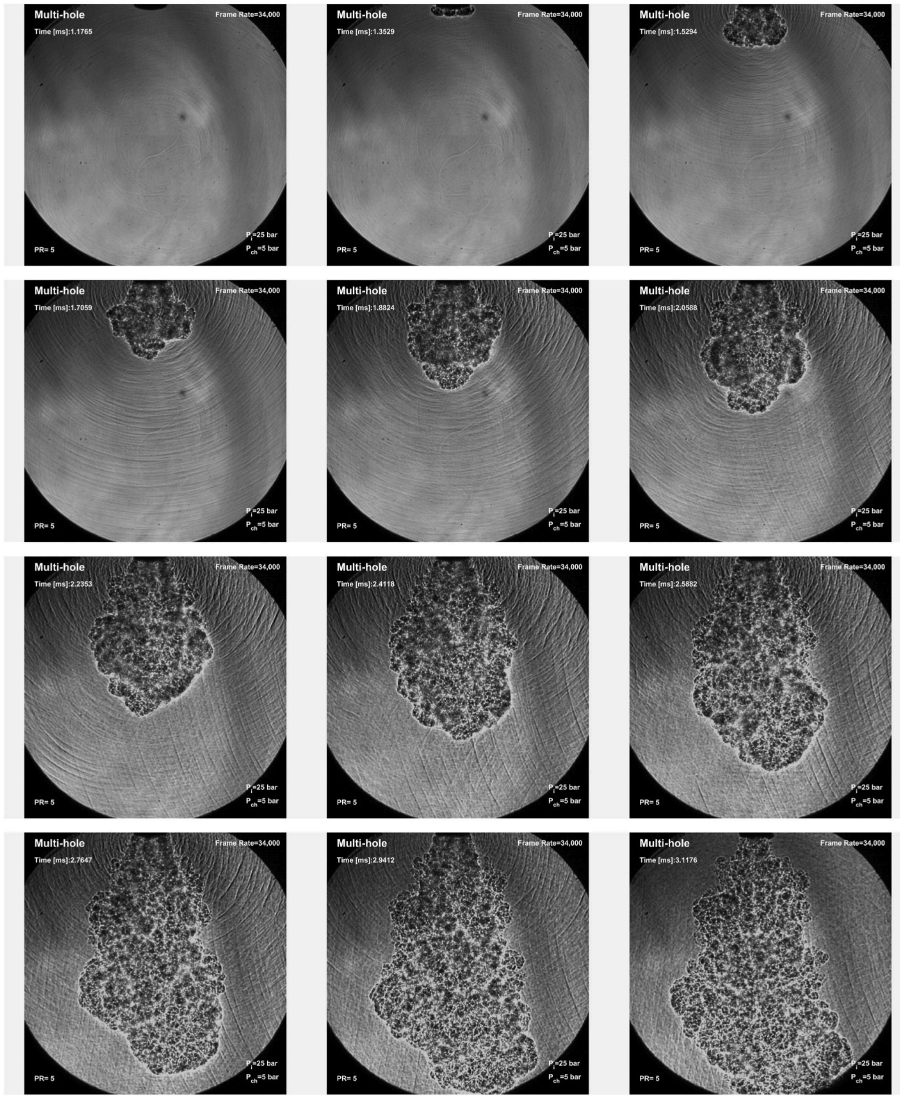

Fig. 6. (*continued*).

the single-hole nozzle, is presented. Lastly, the behavior of the H_2 jet is observed regarding the changes in injection duration (ID).

3.1. Effect of the nozzle geometry and pressure ratio on the H_2 jet characteristics

In this section, a comparative analysis of the jet characteristics is conducted, examining three distinct nozzle configurations (single-hole, double-hole, and multi-hole) at four different pressure ratios (PR = injection pressure (P_i)/chamber pressure (P_{ch}) = 25, 10, 5, and 2.5). These configurations are implemented on the same injector, featuring an outward-opening nozzle.

Fig. 6 illustrates the evolution of the H_2 jets originating from the (a) single-hole, (b) double-hole, and (c) multi-hole nozzles over consecutive time intervals (0.0883 ms for the single-hole, 0.2059 ms for the double-hole, and 0.1764 ms for the multi-hole cases) in the experiments at a constant PR of 5 (P_i = 2.5MPa/P_{ch} = 0.5 MPa)). As it can be observed, the single-hole jet achieves the highest penetration speed, while the double-hole jet trails behind, and the multi-hole jet falls in between. The peak penetration of the jet (which occurs when the jet reaches the bottom edge of the window) for the single-, double-, and multi-hole is at 2.1471 ms, 3.2647 ms, and 2.9412 ms, respectively, after start of energization. Thus, with the single-hole case as the reference, the double-hole jet experiences nearly a 49% delay, while the multi-hole jet lags by around 33% to reach the bottom edge of the window.

Furthermore, while jets from different orifices initially exhibit separation in the vicinity of the nozzle, they appear to recombine further downstream, resulting in jet development resembling that of a single jet with reduced radial expansion. In particular, the double-hole jet exhibits more radial expansion and an effective separation between the two jets, suggesting potential advantages in achieving a more uniform H_2 dispersion within the chamber. These observations are consistent with the results of [56] and quantitatively detailed in the subsequent sections where the jet penetration and cross-sectional area are compared across various nozzle configurations.

For a more comprehensive examination of the influence of nozzle geometry on jet characteristics at different PRs, Fig. 7 provides a detailed view of the jet penetration and cross-sectional area over time for single-hole (SH), double-hole (DH), and multi-hole (MH) nozzles at various PRs (PR = 25, 10, 5, and, 2.5).

As depicted in Fig. 7, irrespective of the PR, the single-hole jet exhibits a swift penetration and the smallest cross-sectional area, while the double-hole jet features the slowest penetration and the largest cross-sectional area. The multi-hole jet falls in between, i.e., with

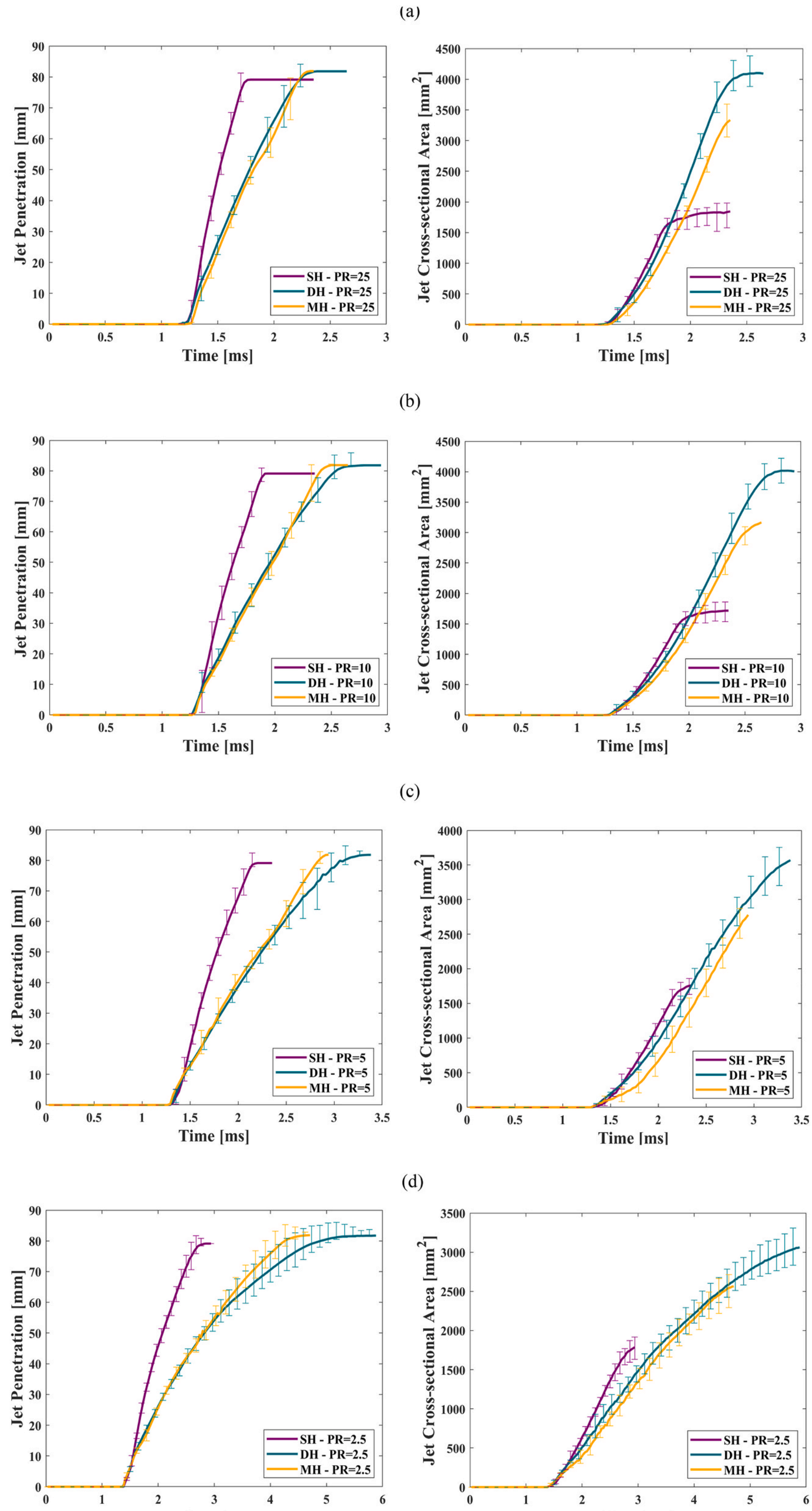

Fig. 7. Comparison of the jet penetration (left) and jet cross-sectional area (right) from the single-hole (SH), double-hole, (DH) and multi-hole (MH) nozzles at PR = 25 (a), 10 (b), 5 (c), and 2.5 (d).

characteristics between those of the single-hole and double-hole jets. The double-hole jet also stands out by possessing a cross-sectional area larger than that of the single-hole and multi-hole jets at a constant PR. This distinction is crucial as it directly enhances air-fuel mixing efficiency, as suggested by prior studies [23,38,40,56]. Therefore, the double-hole nozzle geometry logically emerges as the superior choice for achieving optimal mixing. Table 3 shows the detailed quantitative distinctions among the characteristics of the single-hole, double-hole, and

Table 3
Differences between the H_2 jet characteristics from the single-hole (SH), double-hole, (DH) and multi-hole (MH) nozzles at different PRs.

PR	Nozzle	Maximum jet penetration rate (m/s)	Difference of the jet penetration rate with that of SH as the reference (% slower than SH)	Maximum jet cross-sectional area (mm^2)	Difference of the jet cross-sectional area with that of SH as the reference (% larger than SH)
25	SH	44.2	–	1835.15	–
10	SH	41.37	–	1717.46	–
5	SH	36.56	–	*1753.55*	–
2.5	SH	26.90	–	*1773.03*	–
25	DH	34.33	22.35%	4093.78	123.03%
10	DH	30.47	26.34%	4016.72	133.84%
5	DH	24.40	33.24%	3569.97	103.64%
2.5	DH	13.97	48.03%	3061.45	72.59%
25	MH	35.23	20.27%	3335.17	81.64%
10	MH	33.02	20.17%	3167.44	84.41%
5	MH	28.07	23.24%	2778.5	58.49%
2.5	MH	17.49	34.98%	2559.54	44.38%

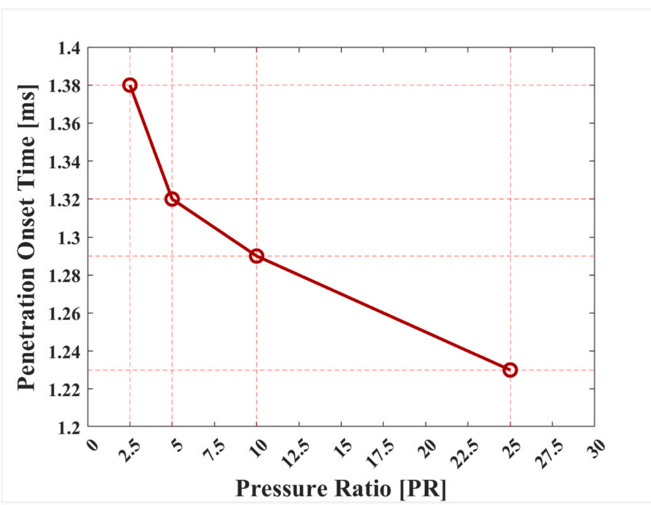

Fig. 8. The injector's valve opening time at different PRs.

multi-hole jets across different PRs.

Another interpretation of Fig. 7 suggests that the increased expansion (cross-sectional area) of the double-hole and multi-hole jets during the free jet development phase cannot be simply attributed to superior jet dispersion within the chamber. Instead, it can be associated with the enhanced air-fuel mixing within the jet possibly due to elevated turbulence levels resulting from jet-to-jet interactions from different nozzle holes as suggested in Ref. [56]. This deduction is supported by the uniform effective nozzle area and consistent injection rate that are integral to the injector's design across all three caps. As a result, the evolution of the equivalence ratio for each nozzle layout at a given PR remains almost identical. Hence, the jet possessing the largest cross-sectional area would present the best uniformity or mixing [56].

In Fig. 7, the effect of PR on the H_2 jet dynamics is also illustrated. PR influences the rate of fuel expansion within a chamber, defining the boundary between the subsonic and supersonic flow regimes. In the current study, all the measurement points fall within the supersonic flow regime since the PRs exceed the minimum threshold for choked conditions [57]. Considering the theoretical limit of choked flow for H_2 at 300 K as PR = 1.89 [18], only the case of PR = 2.5 may not necessarily yield supersonic flow. Hence, because of the choked flow conditions, mass flow is a function of PR and PR can significantly affect turbulence and mixing [57,58]. As it can be observed in Fig. 7, higher PRs (lower P_{ch} as the P_i is constant) lead to increased jet penetration and cross-sectional area, promoting efficient mixing in line with [24,26,38,40,56,59,60].

It is also important to note that this study primarily employs schlieren imaging to monitor jet dynamics, which does not directly yield turbulence structure or fuel concentration for mixing assessment. Nevertheless, the authors have made efforts to evaluate mixture uniformity through parameters like γ as defined in Ref. [24], CFD analysis [56,60], and by analyzing density gradients from pixel grayscale values in the following section. To achieve a more accurate quantification of mixing, the adoption of techniques such as PLIF (planar laser-induced fluorescence) measurements is recommended.

Previously, the authors introduced a parameter, γ, defined as the ratio of injected jet mass (m) to the jet cross-sectional area (A) as a measure of the jet uniformity [24]. In the context of this study, at a constant PR, where the nozzle area and the injected mass are consistent across all the nozzle layouts, the value of γ will be minimized for the double-hole case as it possesses the largest cross-sectional area. This reaffirms the notion that the double-hole cap is preferable at providing the least dense or most uniformly mixed mixture at a constant PR. In addition, the authors developed a CFD model, employing the URANS simulation approach [56,60]. This model assessed mixture uniformity among different nozzle layouts at different PRs and determined that the double-hole nozzle performs best, especially at higher PRs [56].

These results also hold a potential for selection and advancement of optimized nozzle designs aimed at enhancing mixing efficiency. Considering a constant PR, the critical point here is that flow caps featuring multiple nozzle holes with strategically spaced arrangements (such as the double-hole and multi-hole caps in the present study) can facilitate jet-to-jet interactions while maintaining the ability for precise targeting of the fuel to specific regions in the combustion chamber. This presents a challenge that single-hole nozzles typically find difficult to surmount. However, achieving an optimized penetration time (rapid enough penetration) holds an equal significance. This is because the interactions between the jet and the piston constitute another crucial source of turbulent mixing [60]. The relative location of the nozzle holes, specifically the distance between them, can also influence jet behavior, although it has not been investigated in the current work.

As a final note in this section, it should be mentioned that a decrease in PR (equivalently, an increase in P_{ch}) results in a delayed valve opening, which subsequently delays the onset of jet penetration (Fig. 8). The elevated chamber pressure, or increased chamber density, exerts resistance on the injector's valve opening mechanism, subsequently causing a delay in the jet penetration initiation [61]. For the applied injector, this phenomenon is shown in Fig. 8 through a line chart. Upon detailed analysis, it becomes apparent that by considering the minimum P_{ch} = 0.1 MPa as the reference point, an increase to 0.25, 0.5, and 1 MPa results in delays of 4.88%, 7.32%, and 12.20% in the valve opening time (the initiation of jet penetration), respectively. It should be also noted that this delay has been considered in calculating the jet characteristics.

3.2. Impact of the injection angle on the H_2 jet mixing

In the pursuit of addressing another challenge in the development of the next generation of H_2 ICEs, this study also focuses on the influence of injection angle, particularly in the scenario of side-mounted injectors. Since the design of the optical chamber only allows a vertical installation of the injector, an alternative strategy involved using piston bowl profiles with three distinct angles at the bottom of the chamber. This solution enabled the examination of how injection angle impacts jet-piston impingement and mixing.

The interaction between the jet and piston is observed exclusively for the single-hole nozzle configuration at various angles (10°, 15°, and 20°) and PRs (25, 10, 5, and 2.5). Changing the injection angle can lead to jet-piston impingement near the edges of the piston, resulting in an increase

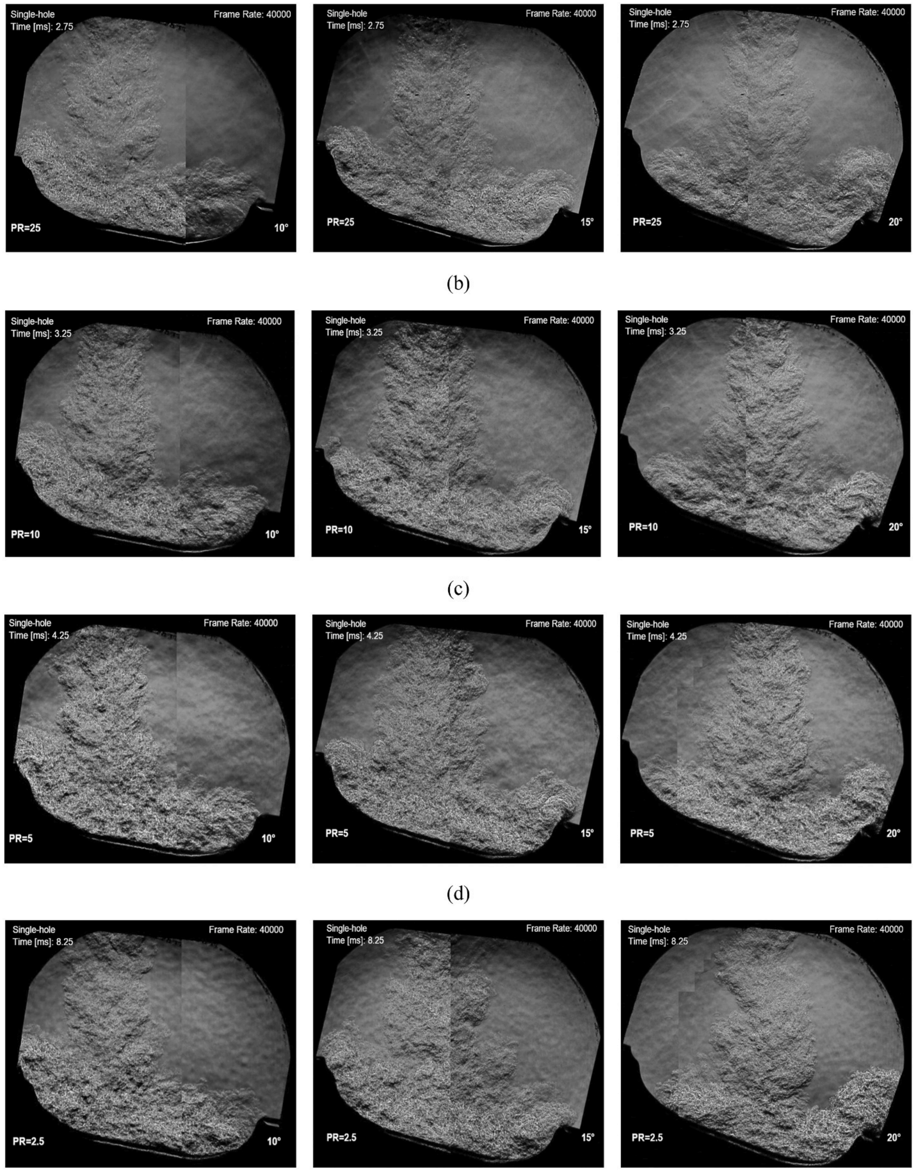

Fig. 9. Injection angle effect on jet-piston impingement for a combined image of one repetition at different PRs = 5 (a),10 (b), 5 (c), and 2.5 (d).

of H_2 concentration in those regions which can adversely affect the uniformity of mixture within the cylinder. It is also a major concern how the in-cylinder flow affects the jet dynamics and mixing in engine applications. However, this aspect has not been investigated in the current study as in-cylinder flow measurements are ideally conducted in an optical engine with a moving piston [60] while the current study involves a constant volume chamber with a stationary piston bowl profile at the bottom of the chamber.

Fig. 9(a–d) demonstrates the influence of injection angle on the jet-piston impingement phase using a combined image from a single repetition across different PRs. Regardless of the PR, it is evident that at the 15° angle, jet-wall impingement occurs near the center of the piston bowl profile, whereas at 10° and 20°, this impingement shifts towards the left and right edges, respectively. Moreover, as observed in Fig. 9, at an injection angle of 20°, a critical deficiency of H_2 on the left liner emerges, as it fails to establish the desired uniformity. In this scenario, fuel congregates predominantly within the central flat region. Simultaneously, there is a notable increase in H_2 concentration along the right liner, ultimately causing an asymmetrical final fuel distribution and the accumulation of fuel within the piston crevice.

In contrast, for the injection angles of 10° and 15°, fuel spreads more symmetrically throughout the piston bowl. For instance, when the injection angle is 15°, the jet initially strikes closer to the piston center and the jet's outline indicates more symmetrical fuel recirculation. Moreover, the recirculating jet on the left side has the potential to interact with the incoming gas flow from the piston, generating additional turbulence. This intriguing effect contributes to enhanced mixing in both the 10° and 15° cases.

In addition, in this study, we assess the mixing phenomenon by generating schlieren signal trajectories that highlight dense regions near the piston edges through pixel grayscale values ranging from 0 to 100 (where 0 representing dark and 100 representing white), constituting a unique aspect of this research (Fig. 10). Initially, an average image is compiled by aggregating data from all repetitions of a case. In the next step, a line is strategically positioned to intersect the target darker regions near the piston edges, where notable density variations, are observed. Following this, grayscale values are recorded and plotted along this line to conduct a quantitative analysis of darker regions signifying higher density gradients (Fig. 11).

Fig. 11 serves as the quantitative companion to Fig. 10, providing insights into the grayscale values along the target lines positioned in Fig. 10. It is worth mentioning that since the images have been merged,

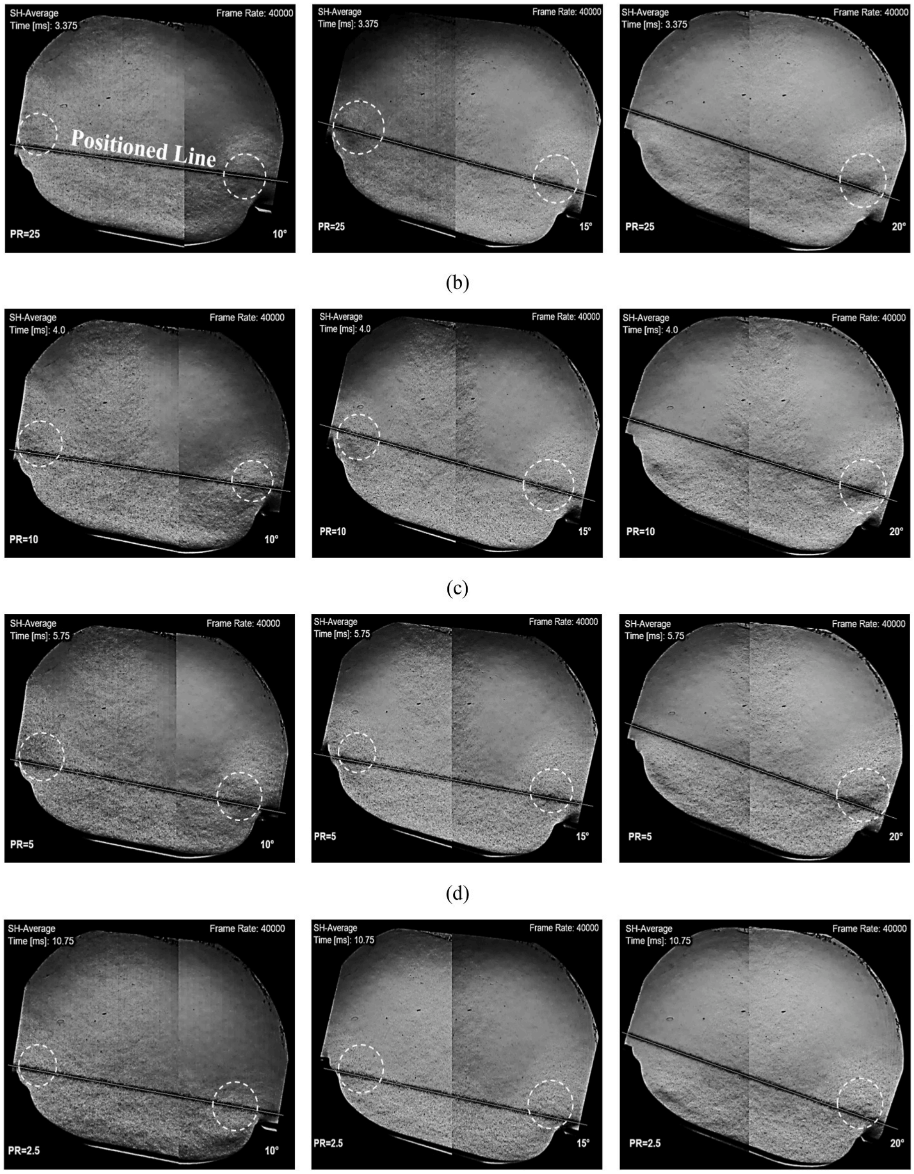

Fig. 10. Injection angle effect on the averaged combined image of jet-piston impingement for 10°, 15°, & 20° at PR = 25 (a), 10 (b), 5 (c), and 2.5 (d). The black positioned line shows the location where the H_2 concentration is further analyzed in Fig. 11 and the dashed white circles show the darker zones near the edges.

the grayscale values between the right and left sides are different as they were not captured simultaneously. To highlight this distinction, a dashed red line symbolizing the division between the right and left sides is featured in Fig. 11. Another important consideration is that, due to the image averaging process, it is expected to observe fluctuations (oscillations) in the grayscale values. However, the primary objective here is to track the overall grayscale pattern and identify areas where abrupt reductions occur, which are indicative of density gradients near the edges.

As depicted in Fig. 10, darker regions near the edges (e.g., those indicated by dashed white circles) result from a high H_2 concentration [60] or vortex formation which is a vital characteristic of impinging jets [62]. The grayscale plots in Fig. 11 quantitatively validate these dark regions by showing reductions in grayscale values marked with dashed red circles, indicating significant density gradients near the piston edges. Given that the most uniform mixtures are characterized by minimal density gradients, the cases displaying subtle grayscale variations excel in achieving superior mixing especially with higher PRs [58,60]. Therefore, according to Fig. 11, as the grayscale difference for the 10° and 15° angle is maximum 20%, whereas for the 20°, is at least 40%, the injection angles of 10° and 15° are more favorable for achieving efficient mixing.

In addition, a CFD model was developed and validated in a previous study by the authors using URANS simulation method to compare fuel distribution across different injection angles [60]. The assessment of a parameter termed “fuel balance” reaffirmed that smaller injection angles, specifically 10° or 15°, may promote a more balanced final mixture, reducing the risk of fuel concentration on the edges of the piston. The interested reader is referred to this work [60] for further detailed information.

3.3. Injection duration effect on the jet characteristics

One of the important parameters that may affect H_2 jet characteristics is the injection duration (ID). In this study, the injection duration defines as the energization time of the solenoid. It plays a pivotal role in regulating injection quantity and, consequently, holds a key role in optimizing engine performance [63]. This optimization is closely tied to the synchronization of valve and ignition timings, which, in turn, significantly influence the heat release process, a critical factor in engine

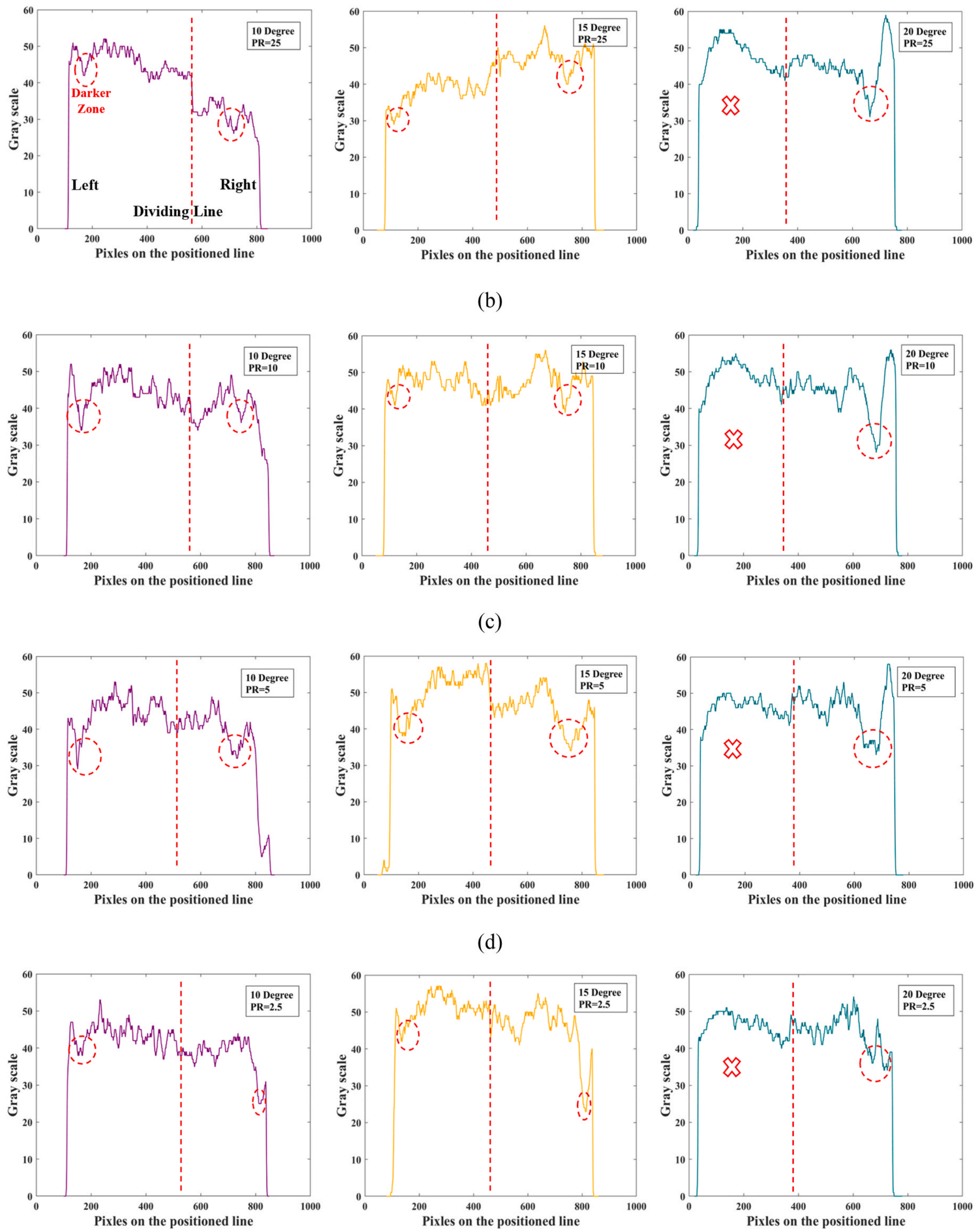

Fig. 11. Counterpart of Fig. 10: grayscale plots of the positioned line on the averaged combined images of 10°, 15°, & 20° at PR = 25 (a), 10 (b), 5 (c), and 2.5 (d). The dashed red line is dividing the right and left sides and the dashed red circles represent the darker regions near the edges where the grayscale of the pixels on the positioned line abruptly drops. (For interpretation of the references to color in this figure legend, the reader is referred to the Web version of this article.)

performance [63]. However, in the case of gas jets, the relationship between their characteristics and the injection duration differs notably from that observed in the context of liquid fuels due to divergent physical properties of gases versus liquids.

In the current experimental campaign, a comprehensive assessment of the impact of injection duration on the H_2 jet characteristics is undertaken. Despite the fundamental importance of injection duration in engine performance, our findings indicate that it does not substantially influence the gas jet characteristics (Fig. 12) which is consistent with other studies e.g., Ref. [64]. Nonetheless, it is imperative to consider the constraints i.e., the limited size of the chamber and field of view. Jet-wall impingement might also occur prior to EOI, suggesting that while conventional jet penetration calculations primarily pertain to the free penetration phase, they may not fully encapsulate all aspects of

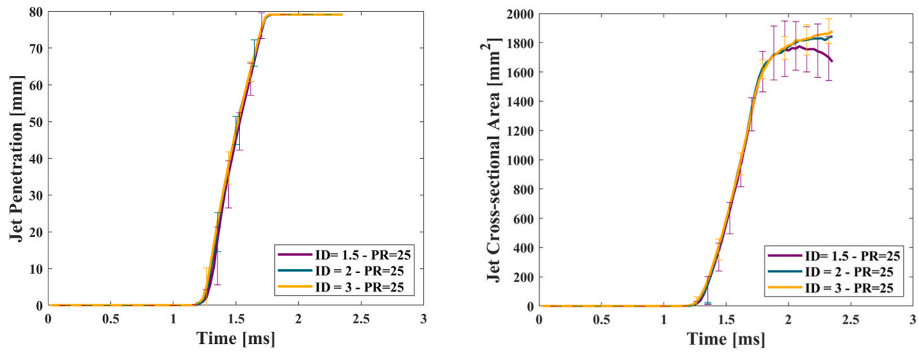

Fig. 12. Effect of injection duration (ID) on the single-hole jet characteristics at PR = 25.

injection duration impact.

In conclusion, the connection between the gas jet characteristics, such as penetration, and injection duration is a multifaceted interplay influenced by several factors encompassing gas properties, initial velocity and momentum, flow rate, nozzle design, and specific applications. Therefore, the optimization of it necessitates a holistic consideration of these factors, alongside a thorough exploration of the potential correlations to the gas jet characteristics.

4. Summary and conclusions

In this paper, experimental investigations of the dynamics of low-pressure H_2 jets using the schlieren imaging technique were conducted to attain better understanding on air-fuel mixing in H_2 DI engines. The H_2 jet characteristics i.e., its penetration and cross-sectional area were studied under the effect of several factors, including nozzle geometry (single-hole, double-hole, and multi-hole), injection angle (10°, 15°, and 20°), pressure ratio (PR, calculated as injection pressure (P_i) divided by chamber pressure (P_{ch})) of 25,10, 5, 2.5, and injection duration (ID). The primary findings can be summarized as follows:

- Regarding the nozzle geometry effect, the single-hole jet displayed the swiftest penetration, trailed by the multi-hole (at least 20.17% slower) and double-hole (at least 22.35% slower). Conversely, the double-hole jet showed advantage in radial development and exhibited a larger cross-sectional area compared to its counterparts (at least 72.59 % larger than the single-hole and 19.62% larger than the multi-hole), leading to enhancement of air-fuel mixture uniformity.
- The interactions between jets in the double-hole and multi-hole nozzles notably improved mixing within the jet. However, when considering a real-world application i.e., a DISI engine, factors such as the timing of fuel injection during the intake stroke should be accounted for. In this context, the multi-hole nozzle might emerge as an appealing choice due to the high diffusivity of H_2 and the balanced compromise it offers between penetration time and cross-sectional area.
- With respect to the injection angle impact on mixing behavior, it was noticed that at 15°, jet-wall impingement occurred closer to the piston bowl's central region, while at 10° and 20°, it shifted towards the left and right edges, respectively. However, a detailed analysis of the schlieren signal trajectories through pixel grayscale values revealed that at smaller injection angles (10° or 15°), fuel dispersed more uniformly across the piston bowl holding promise for improved mixture formation compared to 20°. Nonetheless, it is important to underscore the need for more extensive investigations, including considerations of piston motion and longer mixing durations, to gain deeper insights.
- Concerning the influence of PR on the H_2 jet characteristics, the choked flow phenomenon was observed for all the cases with PR $\geq$ 2.5, resulting in fairly consistent injected mass at various PRs. Additionally, a higher PR denoted a greater pressure gradient from the H_2 jet to the surrounding gas resulting in an extended axial penetration of the jet and a significantly expanded cross-sectional area, resulting in improved mixing efficiency. The findings illustrated that a 50% increase in the PR corresponded to an equivalent 50% expansion in both jet penetration and cross-sectional area. Moreover, it was noted that higher pressure ratios which are correlated with increased turbulence levels and hence, enhanced turbulent mixing, could ultimately yield a more uniform mixture.
- In terms of the impact of Injection Duration (ID) on jet characteristics, our study revealed that it exerted minor influences on the gas jet properties. For instance, negligible difference in jet penetration was noted for injection duration of 1.5, 2, and 3 ms. Nevertheless, it is essential to recognize certain limitations, notably the confined dimensions of the chamber and the restricted 2D field of view.

Based on our findings and the obtained experiences in this work, we suggest that future studies should emphasize optimizing penetration time, ensuring rapid jet penetration. This is crucial as the interaction between the jet and piston plays a pivotal role in turbulent mixing. Therefore, further research exploring flow cap designs (e.g., the effect of distance between nozzle holes on the jet dynamics) to address these aspects is strongly recommended. An appropriate progression would involve continued experimental and numerical investigations with an optical engine and a dynamic piston configuration. For comprehensive examinations of fuel concentration and turbulent mixing, the use of Planar Laser-Induced Fluorescence (PLIF) is proposed.

CRediT authorship contribution statement

Maryam Yeganeh: Formal analysis, Investigation, Software, Validation, Writing – original draft, Writing – review & editing. **Muhammad Saad Akram:** Writing – review & editing. **Qiang Cheng:** Conceptualization, Investigation, Software, Supervision, Writing – review & editing. **Shervin Karimkashi:** Resources, Supervision, Writing – review & editing. **Ossi Kaario:** Resources, Supervision, Writing – review & editing. **Martti Larmi:** Funding acquisition, Supervision, Writing – review & editing.

Declaration of competing interest

The authors declare that they have no known competing financial interests or personal relationships that could have appeared to influence the work reported in this paper.

Acknowledgement

This work was supported by the AGCO Power company and Aalto University School of Engineering Department of Mechanical

Engineering through project no. 410977. Our sincere gratitude extends to MSc. Olli Ranta, MSc. Otto Blomstedt, Senior Technician Jarno Järvinen and B.Sc. Juho Kuusela-Opas for technical assistance and to MSc. Saber Hosseinzade for supporting in data post-processing and analysis. The receipt of the financial support for this research work by Merenkulun säätiö (grant no. 220076 and 20230045), Henry Fordin Säätiö (grant no. 220082 and 20230039), Fortumin ja Nesten Säätiö (grant no.20220165 and 20230111), and Tekniikan Edistamissäätiö (grant no.9501) is also acknowledged.

References

[1] Winkler-Goldstein R, Rastetter A. Power to gas: the final breakthrough for the hydrogen economy? Green 2013;3(1):69–78. https://doi.org/10.1515/green-2013-0001.
[2] Abdalla MA, Hossain S, Nisfindy B, Azad AT, Dawood M, Azad AK. Hydrogen production, storage, transportation, and key challenges with applications: a review. Energy Convers Manag 2018;165:602–27. https://doi.org/10.1016/j.enconman.2018.03.088.
[3] Berry DG, Pasternak AD, Rambach GD, Smith JR, Schock RN. Hydrogen as a future transportation fuel. Energy 1996;21(4):289–303. https://doi.org/10.1016/0360-5442(95)00104-2.
[4] Dennis P, Dingli R, Abbasi Atibeh P, Watson H, et al. Performance of a port fuel injected, spark ignition engine optimized for hydrogen fuel. SAE Technical Paper 2012-01-0654 2012. https://doi.org/10.4271/2012-01-0654.
[5] Huyskens P, Van Oost S, Goemaere P, Bertels K, et al. The technical implementation of a retrofit hydrogen PFI system on a passenger car. SAE Technical Paper 2011-01-2004 2011. https://doi.org/10.4271/2011-01-2004.
[6] Iwasaki H, Shirakura H, Ito A. A study on suppressing abnormal combustion and improving the output of hydrogen fueled internal combustion engines for commercial vehicles. SAE Technical Paper 2011-01-0674 2011. https://doi.org/10.4271/2011-01-0674.
[7] Natarajan S, Abraham M, Rajesh M, Subash G, et al. DelHy 3W - hydrogen fuelled hy-alfa three wheeler. SAE Technical Paper 2013-01-0224 2013. https://doi.org/10.4271/2013-01-0224.
[8] Verhelst S. Recent progress in the use of hydrogen as a fuel for internal combustion engines. Int J Hydrogen Energy 2014;39(2):1071–85. https://doi.org/10.1016/j.ijhydene.2013.10.102.
[9] Koch D, Ebert T, Sousa A. Engine adaptation from diesel to H2 HP-EGR lean combustion concept. MTZ Worldw 2020;81:30–7. https://doi.org/10.1007/s38313-020-0223-9.
[10] Seboldt D, Mansbart M, Grabner P, et al. Hydrogen engines for future passenger cars and light commercial vehicles. MTZ Worldw 2021;82:42–7. https://doi.org/10.1007/s38313-020-0603-1.
[11] Sharma S, Krishna Ghoshal S. Hydrogen the future transportation fuel: from production to applications. Renew Sustain Energy Rev 2015;43:1151–8. https://doi.org/10.1016/j.rser.2014.11.093.
[12] Karimkashi S, Kahila H, Kaario O, Larmi M, Vuorinen V. Numerical study on tri-fuel combustion: ignition properties of hydrogen-enriched methane-diesel and methanol-diesel mixtures. Int J Hydrogen Energy 2020;45:4946–62. https://doi.org/10.1016/j.ijhydene.2019.12.033.
[13] Verhelst S, Turner JWG, Sileghem L, Vancoillie J. Methanol as a fuel for internal combustion engines. Prog Energy Combust Sci 2019;70:43–88. https://doi.org/10.1016/j.pecs.2018.10.001.
[14] Das L, Gulati R, Gupta P. A comparative evaluation of the performance characteristics of a spark ignition engine using hydrogen and compressed natural gas as alternative fuels. Int J Hydrogen Energy 2000;25:783e93. https://doi.org/10.1016/S0360-3199(99)00103-2.
[15] Akansu S, Dulger Z, Kahraman N, Veziroglu T. Internal combustion engines fueled by natural gas and hydrogen mixtures. Int J Hydrogen Energy 2004;29:1527e39. https://doi.org/10.1016/J.IJHYDENE.2004.01.018.
[16] Karim G, Wierzba I, Al-Alousi Y. Methane-hydrogen mixtures as fuels. Int J Hydrogen Energy 1996;21:625e31. https://doi.org/10.1016/0360-3199(95)00134-4.
[17] Thurnheer T, Soltic P, Dimopoulos Eggenschwiler P. S.I.engine fuelled with gasoline, methane and methane/hydrogen blends: heat release and loss analysis. Int J Hydrogen Energy 2009;34:2494–503. https://doi.org/10.1016/j.ijhydene.2008.12.048.
[18] Yip HL, Srna A, Yuen ACY, Kook S, Taylor RA, Yeoh GH, Medwell PR, Chan QN. A review of hydrogen direct injection for internal combustion engines: towards carbon-free combustion. Appl Sci 2019;9:4842. https://doi.org/10.3390/app9224842.
[19] Yu J, Vuorinen V, Kaario O, Sarjovaara T, Larmi M. Visualization and analysis of the characteristics of transitional underexpanded jets. Int J Heat Fluid Flow 2013;44:140–54. https://doi.org/10.1016/j.ijheatfluidflow.2013.05.015.
[20] Kalam M, Masjuki H. An experimental investigation of high-performance natural gas engine with direct injection. Energy 2011;36(5):3563–71. https://doi.org/10.1016/j.energy.2011.03.066.
[21] Li T, Moriwaki R, Ogawa H, Kakizaki R, Murase M. Dependence of premixed low-temperature diesel combustion on fuel ignitability and volatility. Int J Engine Res 2011;13(1):14–27. https://doi.org/10.1177/1468087411422852.
[22] Yu J, Vuorinen V, Kaario O, Sarjovaara, Larmi M. Characteristics of high-pressure jets for direct injection gas engine. SAE Int. J. Fuels Lubr. 2013;6(1):149–56. https://doi.org/10.4271/2013-01-1619.
[23] Kuensch Z, Schlatter S, Keskinen K, Hulkkonen T, Larmi M, Boulouchos K. Experimental investigation on the gas jet behavior for a hollow cone piezoelectric injector. SAE Technical Paper 2014-01-2749 2014. https://doi.org/10.4271/2014-01-2749.
[24] Yeganeh M, Cheng Q, Dharamsi A, Karimkashi S, Kuusela-Opas J, Kaario O, Larmi M. Visualization and comparison of methane and hydrogen jet dynamics using schlieren imaging. Fuel 2023;331(Part 1):125762. https://doi.org/10.1016/j.fuel.2022.125762.
[25] Yu J, Vuorinen V, Kaario O, Sarjovaara T, Larmi M. Visualization and analysis of the characteristics of transitional underexpanded jets. Int J Heat Fluid Flow 2013;44:140–54. https://doi.org/10.1016/j.ijheatfluidflow.2013.05.015.
[26] Wang X, Sun B, Luo Q, Bao L, Su J, Liu J, Li X. Visualization research on hydrogen jet characteristics of an outward opening injector for direct injection hydrogen engines. Fuel 2020;280:118710. https://doi.org/10.1016/j.fuel.2020.118710.
[27] Sankesh D, Petersen P, Lappas P. Flow characteristics of natural-gas from an outward-opening nozzle for direct injection engines. Fuel 2018;218:188–202. https://doi.org/10.1016/j.fuel.2018.01.009.
[28] Duan J, Liu F, Sun B. Backfire control and power enhancement of a hydrogen internal combustion engine. Int J Hydrogen Energy 2014;39(9):4581–9. https://doi.org/10.1016/j.ijhydene.2013.12.175.
[29] Luo QH, Sun BG. Inducing factors and frequency of combustion knock in hydrogen internal combustion engines. Int J Hydrogen Energy 2016;41(36):16296–305. https://doi.org/10.1016/j.ijhydene.2016.05.257.
[30] Chen L, Liang Z, Zhang X, Shuai S. Characterizing particulate matter emissions from GDI and PFI vehicles under transient and cold start conditions. Fuel 2017;189:131–40. https://doi.org/10.1016/j.fuel.2016.10.055.
[31] Ottosson D, Ziori K. Experimental comparison of DI and PFI in terms of emissions and efficiency running Ethanol-85. Master of science thesis MMK 2014:78 MFM 156. KTH Industrial Engineering and Management; 2014. *Machine Design SE-100 44 STOCKHOLM*.
[32] Berg V, Koopmans L, Sjöblom J, Dahlander P. Characterization of gaseous and particle emissions of a direct injection hydrogen engine at various operating conditions. SAE Technical Paper 2023-32-0042 2023. https://doi.org/10.4271/2023-32-0042.
[33] Dober G, Piock W, Meissonnier G, et al. Hydrogen injection systems - a smart path to zero CO2 powertrains. MTZ Worldw 2023;84:28–35. https://doi.org/10.1007/s38313-022-1410-7.
[34] Holtzer BD, Tartakovsky L. Underexpanded impinging gaseous jet interaction with a lubricated cylinder surface. SAE Technical Paper 2023-01-0308 2023. https://doi.org/10.4271/2023-01-0308.
[35] Dober G, Hoffmann G, Doradoux L, et al. Direct injection systems for hydrogen engines. MTZ Worldw 2021;82:60–5. https://doi.org/10.1007/s38313-021-0720-5.
[36] Hu Z, Yuan S, Wei H, Huang Z, Wei H, Chan SH, Zhou L. High-pressure injection or low-pressure injection for a direct injection hydrogen engine? Int J Hydrogen Energy 2024;59:383–9. https://doi.org/10.1016/j.ijhydene.2024.02.018.
[37] Abraham J, Magi V, MacInnes J, Bracco F. Gas versus spray injection: which mixes faster? SAE Technical Paper 940895 1994. https://doi.org/10.4271/940895.
[38] Lee S, Kim G, Bae C. Behavior of hydrogen hollow-cone spray depending on the ambient pressure. Int J Hydrogen Energy 2021;46(5):4538–54. https://doi.org/10.1016/j.ijhydene.2020.11.001.
[39] Lee S, Hwang J, Bae C. Understanding hydrogen jet dynamics for direct injection hydrogen engines. Int J Engine Res 2023;24(10):4433–44. https://doi.org/10.1177/14680874231169562.
[40] Coratella C, Tinchon A, Oung R, Doradoux L, Foucher F. Experimental investigation of the combined impact of backpressure with the pintle dynamic on the hydrogen spray exiting a medium pressure DI outward-opening injector. Int J Hydrogen Energy 2024;49(Part B):432–49. https://doi.org/10.1016/j.ijhydene.2023.08.124.
[41] Zhao J, Liu W, Liu Y. Experimental investigation on the microscopic characteristics of underexpanded transient hydrogen jets. Int J Hydrogen Energy 2020;45(33):16865–73. https://doi.org/10.1016/j.ijhydene.2020.04.140.
[42] Koyanagi K, Hiruma M, Yamane K, Furuhama S. Effect of hydrogen jet on mixture formation in a high-pressure injection hydrogen fueled engine with spark ignition. SAE Technical Paper 931811 1993. https://doi.org/10.4271/931811.
[43] Wallner T, Ciatti S, Bihari B. Investigation of injection parameters in a hydrogen DI engine using an endoscopic access to the combustion chamber. SAE Technical Paper 2007-01-1464 2007. https://doi.org/10.4271/2007-01-1464.
[44] Salazar V, Kaiser S. An optical study of mixture preparation in a hydrogen-fueled engine with direct injection using different nozzle designs. SAE Int. J. Engines 2010;2(2):119–31. https://doi.org/10.4271/2009-01-2682.
[45] Salazar V, Kaiser S, Halter F. Optimizing precision and accuracy of quantitative PLIF of acetone as a tracer for hydrogen fuel. SAE Int. J. Fuels Lubr. 2009;2(1):737–61. https://doi.org/10.4271/2009-01-1534.
[46] Lee S, Kim G, Bae C. Effect of mixture formation mode on the combustion and emission characteristics in a hydrogen direct-injection engine under different load conditions. Appl Therm Eng 2022;209:118276. https://doi.org/10.1016/j.applthermaleng.2022.118276.
[47] Hamzehloo A, Aleiferis PG. Gas dynamics and flow characteristics of highly turbulent under-expanded hydrogen and methane jets under various nozzle pressure ratios and ambient pressures. Int J Hydrogen Energy 2016;41(15):6544–66. https://doi.org/10.1016/j.ijhydene.2016.02.017.

[48] Qu W, Fang Y, Wang Z, Sun H, Feng L. Optimization of injection system for a medium-speed four-stroke spark-ignition marine hydrogen engine. Int J Hydrogen Energy 2022;47(44):19289–97. https://doi.org/10.1016/j.ijhydene.2022.04.096.
[49] Wu B, Torelli R, Pei Y. Numerical modeling of hydrogen mixing in a direct-injection engine fueled with gaseous hydrogen. Fuel 2023;341. https://doi.org/10.1016/j.fuel.2023.127725.
[50] Settles GS. Schlieren and shadowgraph techniques visualizing phenomena in transparent media. first ed. Berlin, Heidelberg: Springer; 2009. https://doi.org/10.1007/978-3-642-56640-0.
[51] National Instruments. "What is LabVIEW?." https://www.ni.com/fi-fi/shop/labview.html#. [accessed 14.December.2023].
[52] PHANTOM. https://www.phantomhighspeed.com/. [accessed 14. December.2023].
[53] Photron Fastcam SA-Z. https://photron.com/fastcam-sa-z2/?gclid=EAIaIQobChMIy87B6K_KgAMV35NoCR3dUQ3BEAAYASAAEgLb6_D_BwE. [Accessed 14 December 2023].
[54] CAVILUX smart for high-speed illumination. https://www.cavitar.com/product/cavilux-smart-for-high-speed-illumination/. [Accessed 14 December 2023].
[55] Wang Z, Bovik AC, Sheikh HR, Simoncelli EP. Image quality assessment: from error visibility to structural similarity. IEEE Trans Image Process 2004;13(4):600–12. https://doi.org/10.1109/TIP.2003.819861.
[56] Yeganeh M, Rabensteiner S, Karimkashi S, Cheng Q, et al. Experimental and numerical study of a low-pressure hydrogen jet under the effect of nozzle geometry and pressure ratio. SAE Technical Paper 2023-01-0320 2023. https://doi.org/10.4271/2023-01-0320.
[57] Vuorinen V, Yu J, Tirunagari S, Kaario O, Larmi M, Duwig C, et al. Large-eddy simulation of highly underexpanded transient gas jets. Phys Fluids 2013;25(1):016101. https://doi.org/10.1063/1.4772192.
[58] Sakellarakis V, Vera-Tudela W, Doll U, Ebi D, Wright Y, Boulouchos K. The effect of high-pressure injection variations on the mixing state of underexpanded methane jets. Int J Engine Res 2021;22(9):2900–18. https://doi.org/10.1177/1468087420960895.
[59] Banholzer M, Vera-Tudela W, Traxinger C, Pfitzner M, Wright Y, Boulouchos K. Numerical investigation of the flow characteristics of underexpanded methane jets. Phys Fluids 2019;31(5):056105. https://doi.org/10.1063/1.5092776.
[60] Yeganeh M, Rabensteiner S, Cheng Q, Ranta O, et al. Experimental and numerical investigation of hydrogen jet-wall impingement. SAE Technical Paper 2022-01-1009 2022. https://doi.org/10.4271/2022-01-1009.
[61] Erfan I, Hajialimohammadi A, Chitsaz I, Ziabasharhagh M, Martinuzzi RJ. Influence of chamber pressure on CNG jet characteristics of a multi-hole high-pressure injector. Fuel 2017;197:186–93. https://doi.org/10.1016/j.fuel.2017.02.018.
[62] Yu J, Vuorinen V, Hillamo H, Sarjovaara T, Kaario O, Larmi M. An experimental investigation on the flow structure and mixture formation of low pressure ratio wall-impinging jets by a natural gas injector. J. Nat. Gas Eng. 2012;9:1–10. https://doi.org/10.1016/j.jngse.2012.05.003.
[63] Aljamali S, Abdullah S, Wan Mahmood WMF, Ali Y. The effect of injection timings on performance and emissions of compressed natural-gas direct injection engine. J. Combust. 2016:7. https://doi.org/10.1155/2016/6501462. Article ID 6501462.
[64] Borz M, Kim Y, O'Connor J. The effects of injection timing and duration on jet penetration and mixing in multiple-injection schedules. SAE Technical Paper 2016-01-0856 2016. https://doi.org/10.4271/2016-01-0856.